3D Imaging and Manipulation of Subsurface Selenium Vacancies in PdSe_{2}

Giang D. Nguyen, Liangbo Liang, Qiang Zou, Mingming Fu, Akinola D. Oyedele, Bobby G. Sumpter, Zheng Liu, Zheng Gai, Kai Xiao, and An-Ping Li

Phys. Rev. Lett. **121**, 086101 — Published 20 August 2018

DOI: 10.1103/PhysRevLett.121.086101

3D imaging and manipulation of subsurface selenium vacancies in $PdSe_2$

Giang D. Nguyen,[1] Liangbo Liang,[1,*] Qiang Zou,[1] Mingming Fu,[1] Akinola D. Oyedele,[1,2] Bobby G. Sumpter,[1,3] Zheng Liu,[4] Zheng Gai,[1] Kai Xiao[1], An-Ping Li[1,*]

[1]*Center for Nanophase Materials Sciences, Oak Ridge National Laboratory, Oak Ridge, Tennessee 37831, United States*

[2]*Bredesen Center for Interdisciplinary Research and Graduate Education, University of Tennessee, Knoxville, Tennessee 37996, United States*

[3]*Computational Sciences & Engineering Division, Oak Ridge National Laboratory, Oak Ridge, Tennessee 37831, United States*

[4]*Center for Programmable Materials, School of Materials Science & Engineering, Nanyang Technological University, Singapore 639798, Singapore*

ABSTRACT

Two-dimensional materials such as layered transition-metal dichalcogenides (TMDs) are ideal platforms for studying defect behaviors, an essential step towards defect engineering for novel material functions. Here we image the 3D lattice locations of selenium vacancy (V_{Se}) defects and manipulate them using a scanning tunneling microscope (STM) near the surface of $PdSe_2$, a recently discovered pentagonal layered TMD. The V_{Se} show a characterisitc charging ring in spatially resolved conductance map, based on which we can determine its subsurface lattice location precisely. Using the STM tip, not only can we reversibly switch the defect states between charge neutral and charge negative, but also trigger migrations of V_{Se} defects. This allows a demonstration of direct "writing" and "erasing" of atomic defects and tracing the diffusion

pathways. First-principles calculations reveal a small diffusion barrier of V_{Se} in $PdSe_2$ which is much lower than S vacancy in MoS_2 or an O vacancy in TiO_2. This finding opens an opportunity of defect engineering in $PdSe_2$ for such as controlled phase transformations and resistive-switching memory (RRAM) device application.

PACS numbers: 68.37.Ef, 67.80.Mg

Vacancy defects play a significant role in determining the physical properties of crystalline materials. Most notably, a charge neutral vacancy (V^0) can capture an electron (V^-) or emit an electron (V^+) to become charge states, and each of these states will introduce a different type of dopant in semiconductors. Understanding vacancy behaviors constitutes a significant step in defect engineering that not only modifies the conductance of semiconductors, but also enables novel material functions ranging from high-spin states such as nitrogen-vacancy centers in diamond [1], ionic diffusion path enabled by oxygen-vacancies in perovskite [2], and catalytic sites introduced by sulfur vacancies in MoS_2 [3]. Therefore, controling vacancy defects, especially the ability of reverably manipulating vacancies at the atomic level, has become a promising approach to defect engineering and novel material functions [4-8]. As an example, Yang et al. demonstrated a memristor operation by controling the migration of oxygen vacancy in TiO_2 under an applied electric field, but the precision of control was limited to the size of the device on a 50 nm scale [2]. Using an STM tip, Setvin et al. were able to pull oxygen vaccancies to the surface with a high bias voltage (~5 V) to alter the surface properties of TiO_2 [9], but a reverable process remains to be demonstrated. Recently, the advent of 2D materials have attracted great research interests on vacancy defects in graphene and transition metal dichalcogenites (TMDs) [3, 10, 11]. For example,

Sangwan et al. reported a gate-tunable memristive behavior based on control of defect migration at grain boundary in MoS_2 [12]. However, there has been no report on atomic control of the vacancy diffusion process in 2D materials.

$PdSe_2$, a newly discovered pentagonal TMD [13-16], has recently attracted vibrant research interest due to the extraordinary high carrier mobility [13] and air-stability [15] that are desirable for 2D electronic applications. In contrast to the frequently reported hexagonal phases in layered TMDs, $PdSe_2$ has an uncommon pentagonal network with a puckered lattice structure. Each $PdSe_2$ slab consists of a Se-Pd-Se trilayer where each Pd atom is bonded to four Se atoms located on the top and bottom sublayers [15] as illustrated in Fig. 1(a). The two Se atoms located in the top and bottom sublayers form a tilted Se-Se dumbbell crossing the Pd layer, resulting in a lack of rotational symmetry. Such structure is potentially sensitive to defects, as Se vacancy (V_{Se}) would break the symmetry of the Se-Se dumbbell and induce large structural distortion [14]. This contrasts with the commonly observed layered hexagonal TMDs, where the lattice remains intact even at a relatively high concentration of chalcogen vacancy [17].

In this letter, we report on imaging and manipulation of individual Se vacancies V_{Se} in $PdSe_2$ using an STM. By imaging the characteristic charge rings of defects arising from a tip-induced band bending (TIBB) effect [4-8, 18-22], we first determine the 3D lattice locations of V_{Se} precisely in the subsurface region. We then demonstrate the use of an STM tip as a movable electrostatic gate to manipulate V_{Se} by reversibly switching the charge states of defects between neutral V^0 and negative V^- states. We find a relatively small bias voltage (~2.0 V) at the STM tip can be used to trigger vacancy migrations, which allows us to demonstrate both direct "writing" and "erasing" of atomic defects in $PdSe_2$ while tracing their diffusion pathways. The results are corroborated by first-principles calculations that reveal the formation energy and diffusion barriers

of Se vacancies in $PdSe_2$. This work opens an opportunity for defect engineering in $PdSe_2$ at the atomic level to achieve controlled phase transformations [14, 23] or new material functions such as resistive switching memory (RRAM) [12, 24-27].

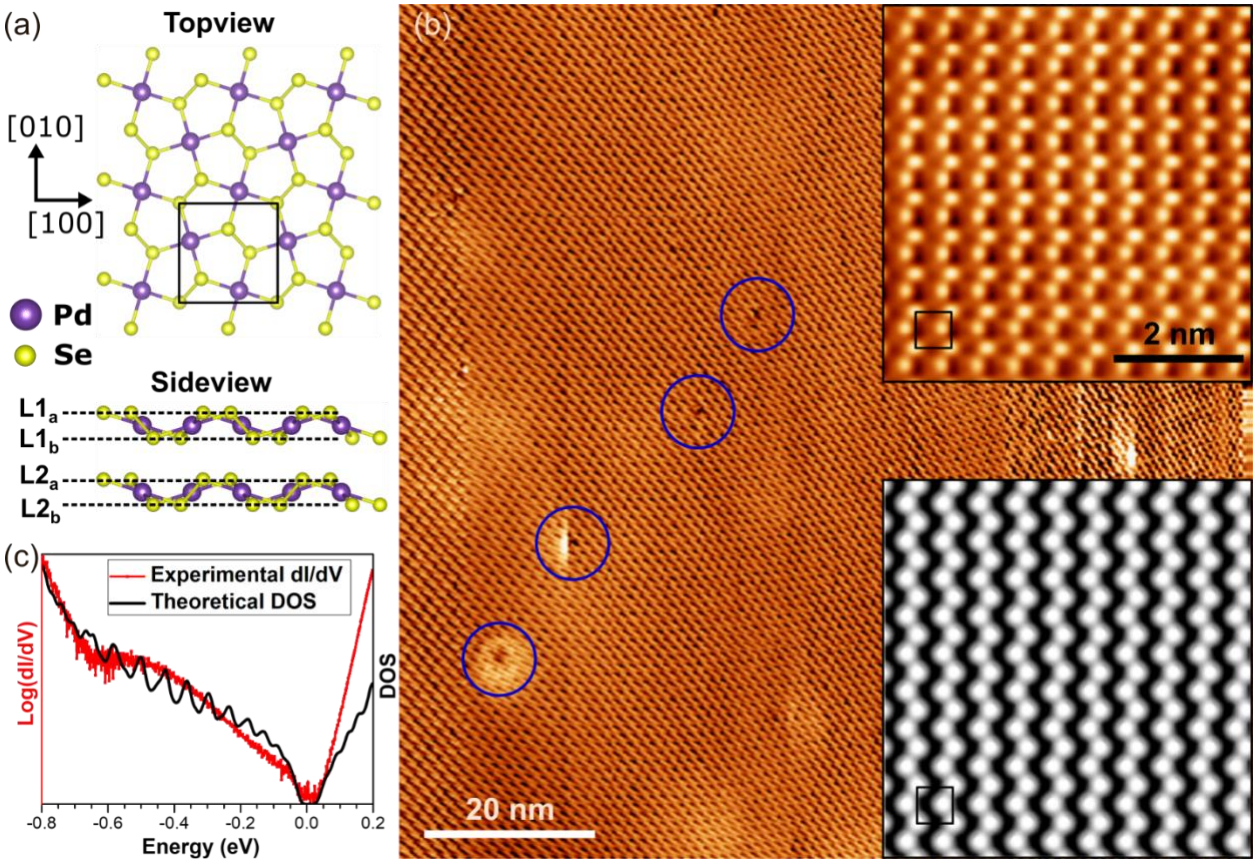

FIG. 1: *Probing the structure and bandgap on $PdSe_2$ surface.* (**a),** Sketch of the crystallographic structure of $PdSe_2$ with the purple and yellow spheres representing the Pd and Se atoms, respectively. $L1_a$, $L1_b$,… define Se sublayers along [001] direction where the Se top surface layer is counted as layer $L1_a$. (b)**,** A typical STM topographic image of $PdSe_2$, blue circles indicate some V_{Se} defects (sample bias $V_s = -1.0$ V, tunneling current $I = 50$ pA, temperature $T = 120$ K). The inset in (b) shows the atomically resolved STM image (top right corner, Fourier filtering was applied to enhance the contrast) and simulated image (bottom right corner) of $PdSe_2$ at 0.3 V. (c)**,**

dI/dV spectrum on $PdSe_2$ in comparison with theoretical density of states (DOS) of $PdSe_2$ (V_s = −0.9 V, I = 3 nA, V_{ac} = 10 mV, f = 1000 Hz, T = 120 K).

Here, we study the behaviors of individual defects by visualizing and manipulating V_{Se} in bulk $PdSe_2$ with STM. $PdSe_2$ single crystals were synthesized by a self-flux method as previously reported [15]. A bulk crystal of $PdSe_2$ was cleaved along [001] direction *in situ* in ultra-high vacuum at room temperature. Figure 1(b) shows a typical STM image of cleaved $PdSe_2$ surface. The atomically resolved STM image (upper inset of Fig. 1(b)) shows a square network with lattice constants of 0.58 ± 0.01 nm, and bright spots visualizing the Se atoms on the topmost sublayer. A simulated image (lower inset of Fig. 1(b)) is in excellent agreement with the STM image, corroborating this interpretation. $PdSe_2$ has an orthorhombic unit cell with in-plane lattice constants of a ≈ 0.575 nm and b ≈ 0.587 nm [28], and its in-plane unit cell is very close to the square network shown in Fig. 1(b) after considering experimental uncertainty. Figure 1(c) shows the measured dI/dV spectrum (red curve) with a bandgap 0.06 ± 0.02 eV (see Fig. S1 for more details [29] with Refs. [30-32]). This measured bandgap is corroborated by calculated density of states (DOS) (black curve in Fig. 1(c)) using density functional theory (DFT) with the many-body *GW* approximation. Individual V_{Se} defects on $PdSe_2$ can be visualized by STM images. Defects on the top surface are shown as dark holes which indicates the missing of Se surface atoms (blue circles in Fig. 1(b)). This observation confirms the existence of V_{Se} in $PdSe_2$ as reported previously [14]. The V_{Se} introduces unoccupied in-gap states (Fig. S2) that can be revealed as alternative dark and bright contrast when varying sample bias from positive to negative values (see Fig. S3 for more details [29]).

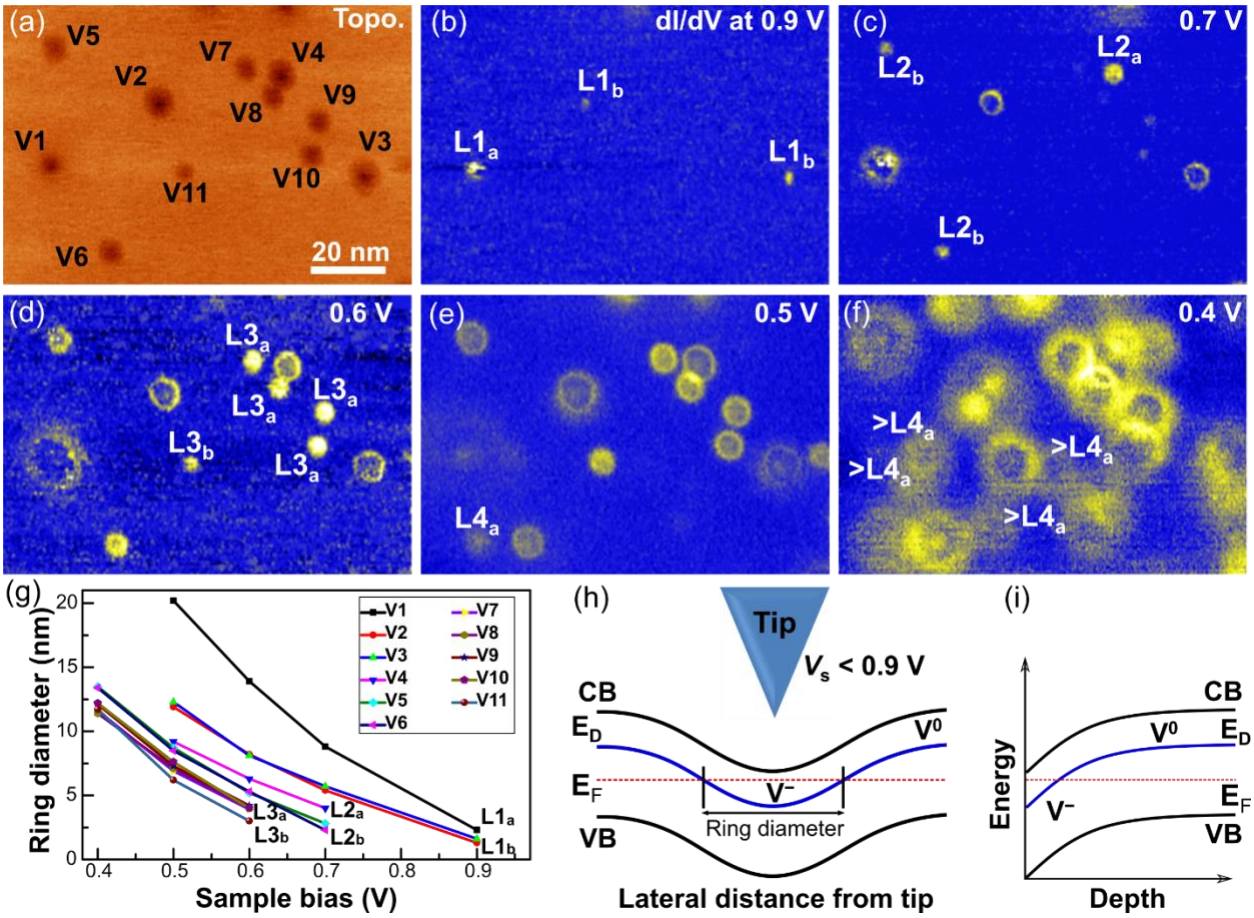

FIG. 2: *Imaging Se vacancy defects and switching charge state of the defects in $PdSe_2$.* (a) STM topographic image showing V_{Se} defects as dark disks and labeled as V1 to V11 (V_s = 0.5 V, I = 50 pA, T = 120 K). (b)-(f) The evolution of measured differential conductance dI/dV map as a function of sample bias, showing defects located on different lattice layers as rings of different diameters. (g) The dependence of ring diameter as a function of sample bias for 11 defects. (h) A sketch of the lateral tip-induced band bending on the sample below the STM tip showing the switch of charge neutral V^0 to negative state V^-. (i) A sketch of depth-dependent band bending of conduction band (CB), valence band (VB), and defect state (E_D) below the tip position.

We now examine V_{Se} defect behaviors. Figure 2(a) shows a STM topographic image on an area with eleven V_{Se} defects labeled numerically. In the spatially resolved differential conductance d*I*/d*V* maps (Figs. 2(b)-(f)), these defects appear as a ring-like feature in the sample bias range of 0.9 V to 0.4 V. At a constant bias voltage below the threshold, a higher tunneling current leads to a larger ring (Fig. S4 [29]). This result indicates that the ring size actually varies with the tip-sample distance in which a farther separation results in a smaller ring (Fig. S4(f)). These observations suggest that the ring features in d*I*/d*V* maps do not correlate with the local DOS; instead they can be explained as defect charge states due to tip-induced band bending (TIBB) effect [33]. Similar features were previously observed in doped semiconductors GaAs [34] and InAs [18], Co-adatoms in graphene[35], vacancies in black phosphorous [22], Fe dopants in Bi_2Se_3 [36] . The switch of charge state gives rise to the ring feature in d*I*/d*V* maps, which occurs at a specific voltage when the dopant level crosses the bulk Fermi level (Fig. 2(h)) [18, 22, 34]. In such a process, larger rings are expected for a smaller sample bias and smaller tip-sample separation (larger TIBB). Therefore, depending on the sample bias, the STM tip can switch reversibly the charge states of an individual V_{Se} defect in $PdSe_2$ between V^0 and V^- (Fig. S5 [29]).

Figure 2(g) shows the change of ring diameter as a function of the sample bias voltage for the 11 defects labeled in Fig. 2(a). The charging rings become smaller as bias voltage approaches the threshold, corroborating a TIBB process. At the same bias voltage, different ring sizes indicate the different depths of these defects from the surface of $PdSe_2$. The defects located at a deeper layer have smaller TIBB (Fig. 2(i)), and thus their rings are smaller. Moreover, defects deeper below the surface have a lower charging threshold, which is clearly seen in the d*I*/d*V* maps shown in Figs. 2(b)-(f). Based on this information, we can assign V_{Se} defects to individual Se sublayers as shown in Figs. 2(b)-(g), although the assignment for deeper than the 3rd layer (L3) is less

accurate due to the limit of statistical data. The onset voltage of charging ring of defects in the two sublayers of the same $PdSe_2$ slab is almost the same, e.g., 0.9 V for $L1_a$ and $L1_b$, 0.7 V for $L2_a$ and $L2_b$, and 0.6 V for $L3_a$ and $L3_b$. This is simply because the distance between two Se sublayers in one $PdSe_2$ slab is smaller compared to the distance between two adjacent Se sublayers at two $PdSe_2$ slabs [15]. Therefore, the STM tip not only allows us to reversibly switch the charge state of a V_{Se} defect, but also enables us to identify the location of the defects in the subsurface atomic lattice. It provides us a capability for precise 3D imaging of individual defects in a crystalline lattice, especially in 2D layered materials where their atomic layers are well separated.

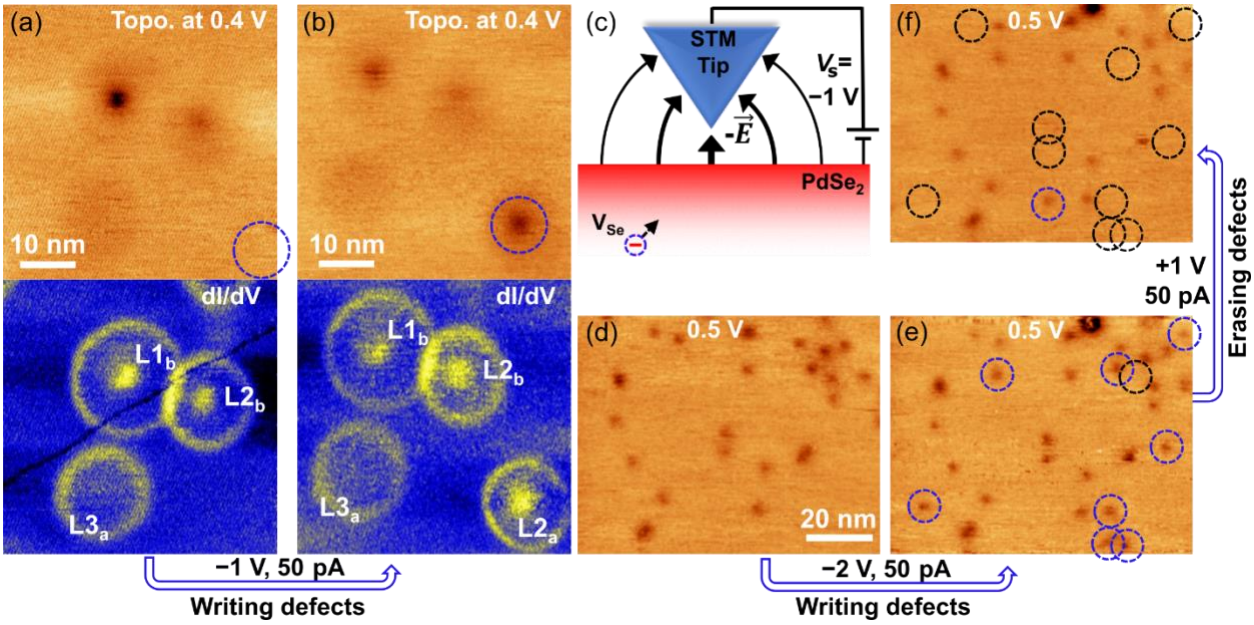

FIG. 3: *Manipulation of Se vacancy defects by an STM tip***.** (a), (b) STM topographic images (upper panel) and d*I*/d*V* maps (lower panel) before (a) and after (b) treating the sample area with an STM tip by scanning at $V_s = -1.0$ V, $I = 50$ pA. The images and d*I*/d*V* maps are acquired at $V_s = 0.4$ V, $I = 50$ pA, $V_{ac} = 50$ mV, $f = 1000$ Hz, $T = 120$ K. (c) Schematic illustrating V_{Se} migration to underneath the STM tip induced by the electrical field from the STM tip. (d)-(f) V_{Se} defects induced and removed on the surface after treating the surface by scanning at −2 V and +1 V,

respectively. The images are acquired at V_s = 0.5 V, I = 50 pA, T = 120 K. Blue dashed circles mark the new defects; black circles indicate defect disappearance.

We now try to manipulate V_{Se} by changing its lattice locations with the STM tip. Figure 3(a) shows three V_{Se} located respectively on lattice layers $L1_b$, $L2_b$, and $L3_a$ according to the sizes of their charge rings and voltage thresholds (the complete set of dI/dV maps at different biases in Fig. S6). A new V_{Se} defect emerges on layer $L2_a$, as shown in Fig. 3(b), after scanning the area with a high negative sample bias (−1 V with a tunneling current of 50 pA). We believe that the STM tip at negative sample bias trigger V_{Se} migration to underneath the tip during scanning as illustrated in Fig. 3(c). This hypothesis is corroborated with a controlled experiment. Figure 3(d) is an STM image acquired at a normal condition of V_s = 0.5 V, I = 50 pA, showing V_{Se} defects as dark spots. The same area of the $PdSe_2$ surface is then treated by STM scanning with a high negative bias at −2 V, 50 pA. Figure 3(e) is then acquired with the normal condition, which contains new V_{Se} defects in the sample area as marked by dashed blue circles. Most of these defects disappear after a reverse treatment with a high positive sample bias (1 V, 50 pA), as marked by dashed black circles in Fig. 3(f). This kind of tip-induced vacancy "writing and erasing" process is similar to that observed recently in oxygen vacancies (V_O) in TiO_2 [9, 37], although a significantly higher bias (5.2 V) was required for moving V_O and only "writing" process was demonstrated in TiO_2 with the STM tip. It is noted that the field-induced migration of V_O in metal oxides is already applied in novel resistive memory device applications [2, 27]. Our result shows that 2D materials like $PdSe_2$ can be next generation materials for the memory device with much lower energy consumption and higher efficiency.

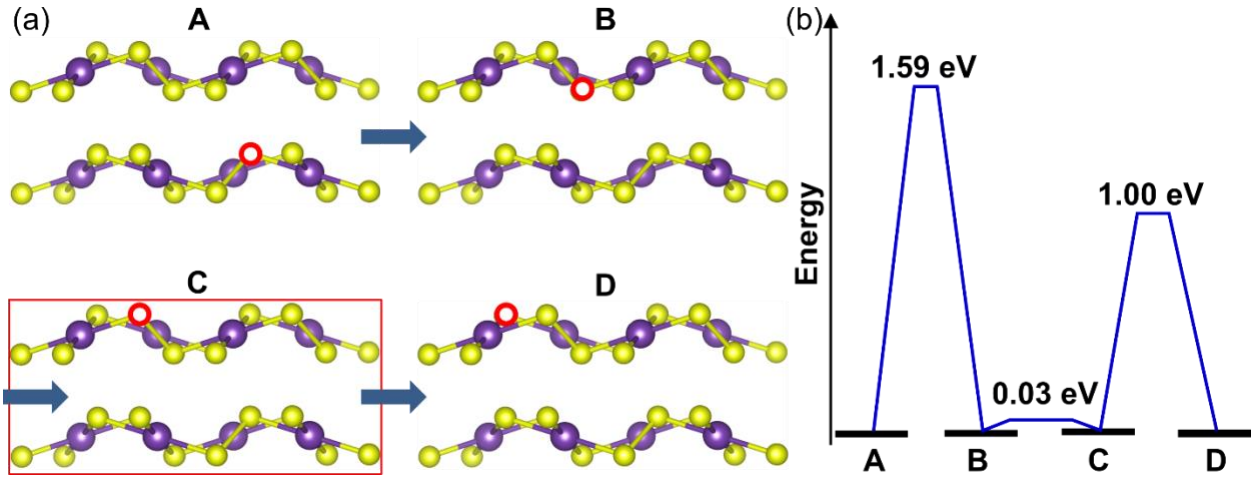

FIG. 4: *Se vacancy diffusion between two layers or within the same layer***.** (a) Schematic of different V_{Se} configurations in the $PdSe_2$ sample, with red circle marking the V_{Se} site. (b) Calculated energy barriers for V_{Se} diffusion between the different defect configurations.

To understand the tip-induced V_{Se} migration in $PdSe_2$, we calculated the energy barriers for V_{Se} diffusion between two layers (interlayer) or within the same layer (intralayer) using the climbing image nudged elastic band (CI-NEB) method [38]. The nudged elastic band (NEB) method finds saddle points and minimum energy paths between the initial and final states, by optimizing a number of intermediate images along the reaction path (see more details in Supplemental Material [29] with additional Refs. [38-43]). The four possible configurations for V_{Se} positions (marked with red circles) are sketched and labeled as A, B, C, and D in Fig. 4a. The corresponding energy barriers for the diffusion of a V_{Se} between these configurations are shown in Fig. 4(b). The relaxed atomic structures for these four configurations and the corresponding transition states are shown in Fig. S7 [29]. The energy barrier is 1.59 eV for the interlayer V_{Se} diffusion from configuration A to B. In comparison, we performed a similar calculation for S vacancy (V_S) in MoS_2 and find a much higher barrier of 4.44 eV for the similar interlayer V_S

diffusion in MoS_2. This significant difference can be attributed to the fact that the interlayer binding energy in $PdSe_2$ is notably larger than that in MoS_2, and the average interlayer distance in $PdSe_2$ is much shorter than that in MoS_2 [15, 44, 45]. Furthermore, for the intralayer V_{Se} diffusion in $PdSe_2$ from configuration C to D, the energy barrier is computed to be around 1 eV, which is also much lower than the barrier (2.30 eV) for the corresponding intralayer V_S diffusion in MoS_2 [46]. Compared to hexagonal MoS_2, the unique pentagonal network with relatively weaker covalent bond strength in $PdSe_2$ facilitates the V_{Se} migration. Finally, almost no barrier (0.03 eV) exists for the intralayer V_{Se} diffusion from configuration B to C, i.e., from the bottom Se sublayer to the top Se sublayer (Fig. 4(a)), due to the covalent bond between these two Se atoms (also see Fig. S7 [29]). In short, unlike the well-known MoS_2, the V_{Se} diffusion in $PdSe_2$ is considerably easier. This is consistent with an additional experiment where we find that V_{Se} can easily diffuse both vertically and laterally in the $PdSe_2$ at the room temperature even when scanning at relatively low sample bias of 0.4 V (Fig. S8). Thus, a STM tip can be used both to trigger vacancy migration and to trace the pathways of vacancy diffusion. However, in our experiment, we often observed the diffusion of a Se vacancy in about 10 nm. It must consist of multiple movement steps.

In conclusion, we have shown how an STM can be used for 3D imaging and manipulation of individual V_{Se} defects in $PdSe_2$. The V_{Se} is shown as circular ring feature in spatially resolved conductance map whose diameter changes in response to a TIBB effect. Based on the behaviors of this charging ring, the subsurface lattice location of V_{Se} can be precisely determined. The TIBB can be further utilized to reversibly switch the defect from charge neutral to charge negative states. Moreover, the electrical field from an STM tip can induce migrations of vacancies, which allows direct “writing” and “easing” of atomic defects and tracing the diffusion pathways of V_{Se}. The diffusion kinetic barrier of V_{Se} in $PdSe_2$ is much lower than V_O in TiO_2 or V_S in MoS_2, paving the

way for manipulating the V_{Se} in $PdSe_2$ in defect engineering for novel functionalities, such as controlled phase transformations [14, 23] and memory device application [12, 24-27].

Acknowledgement

This research was conducted at the Center for Nanophase Materials Sciences, which is a DOE Office of Science User Facility. L.L. was supported by Eugene P. Wigner Fellowship at the Oak Ridge National Laboratory (ORNL). Part of the computations was performed using the resources of the Center for Computational Innovation at Rensselaer Polytechnic Institute.

Corresponding authors: An-Ping Li (apli@ornl.gov) and Liangbo Liang (liangl1@ornl.gov)**.**

References

[1] L. Childress, M. G. Dutt, J. Taylor, A. Zibrov, F. Jelezko, J. Wrachtrup, P. Hemmer, and M. Lukin, Science 314, 281 (2006).
[2] J. J. Yang, M. D. Pickett, X. Li, D. A. Ohlberg, D. R. Stewart, and R. S. Williams, Nature nanotechnology 3, 429 (2008).
[3] D. Le, T. B. Rawal, and T. S. Rahman, The Journal of Physical Chemistry C 118, 5346 (2014).
[4] D. Eom, E. Seo, and J.-Y. Koo, Physical Review B 94, 195308 (2016).
[5] D.-H. Lee and J. A. Gupta, Nano letters 11, 2004 (2011).
[6] H. Liu, H. Zheng, F. Yang, L. Jiao, J. Chen, W. Ho, C. Gao, J. Jia, and M. Xie, ACS Nano 9, 6619 (2015).
[7] J. Riffle, C. Flynn, B. St. Laurent, C. Ayotte, C. Caputo, and S. Hollen, Journal of Applied Physics 123, 044301 (2018).
[8] H. Zheng, A. Weismann, and R. Berndt, Physical Review letters 110, 226101 (2013).
[9] M. Setvín, U. Aschauer, P. Scheiber, Y.-F. Li, W. Hou, M. Schmid, A. Selloni, and U. Diebold, Science 341, 988 (2013).
[10] S. M. Hus and A.-P. Li, Progress in Surface Science 92, 176 (2017).
[11] S. Zhang, C.-G. Wang, M.-Y. Li, D. Huang, L.-J. Li, W. Ji, and S. Wu, Physical Review letters 119, 046101 (2017).
[12] V. K. Sangwan, D. Jariwala, I. S. Kim, K.-S. Chen, T. J. Marks, L. J. Lauhon, and M. C. Hersam, Nature Nanotechnology 10, 403 (2015).
[13] W. L. Chow *et al.*, Advanced Materials 29, 1602969 (2017).
[14] J. Lin, S. Zuluaga, P. Yu, Z. Liu, S. T. Pantelides, and K. Suenaga, Physical Review Letters 119, 016101 (2017).
[15] A. D. Oyedele *et al.*, Journal of the American Chemical Society 139, 14090 (2017).

[16] M. A. ElGhazali, P. G. Naumov, H. Mirhosseini, V. Süß, L. Müchler, W. Schnelle, C. Felser, and S. A. Medvedev, Physical Review B 96, 060509 (2017).
[17] M. Mahjouri-Samani *et al.*, Nano Letters 16, 5213 (2016).
[18] F. Marczinowski, J. Wiebe, J.-M. Tang, M. Flatté, F. Meier, M. Morgenstern, and R. Wiesendanger, Physical Review Letters 99, 157202 (2007).
[19] F. Marczinowski, J. Wiebe, F. Meier, K. Hashimoto, and R. Wiesendanger, Physical Review B 77, 115318 (2008).
[20] N. Pradhan, N. Liu, C. Silien, and W. Ho, Physical Review Letters 94, 076801 (2005).
[21] A. Wijnheijmer, J. Garleff, K. Teichmann, M. Wenderoth, S. Loth, R. Ulbrich, P. Maksym, M. Roy, and P. Koenraad, Physical Review Letters 102, 166101 (2009).
[22] Z. Qiu *et al.*, Nano Letters 17, 6935 (2017).
[23] S. Bordier, A. Chocard, and S. Gossé, Journal of Nuclear Materials 451, 120 (2014).
[24] H.-S. P. Wong, H.-Y. Lee, S. Yu, Y.-S. Chen, Y. Wu, P.-S. Chen, B. Lee, F. T. Chen, and M.-J. Tsai, Proceedings of the IEEE 100, 1951 (2012).
[25] R. Ge, X. Wu, M. Kim, J. Shi, S. Sonde, L. Tao, Y. Zhang, J. C. Lee, and D. Akinwande, Nano Letters 18, 434 (2018).
[26] V. K. Sangwan, H.-S. Lee, and M. C. Hersam, in *Electron Devices Meeting (IEDM), 2017 IEEE International* (IEEE, 2017), pp. 5.1. 1.
[27] A. Sawa, Materials Today 11, 28 (2008).
[28] C. Soulard, X. Rocquefelte, P.-E. Petit, M. Evain, S. Jobic, J.-P. Itie, P. Munsch, H.-J. Koo, and M.-H. Whangbo, Inorganic Chemistry 43, 1943 (2004).
[29] See Supplemental Material at [URL] for detailed methods on theoretical calculations and additional data, which incluides Refs. [30-32].
[30] C. Domke, P. Ebert, and K. Urban, Surface Science 415, 285 (1998).
[31] S. Haldar, H. Vovusha, M. K. Yadav, O. Eriksson, and B. Sanyal, Physical Review B 92, 235408 (2015).
[32] S. Loth, M. Wenderoth, K. Teichmann, and R. Ulbrich, Solid State Communications 145, 551 (2008).
[33] R. M. Feenstra and J. A. Stroscio, Journal of Vacuum Science & Technology B: Microelectronics Processing and Phenomena 5, 923 (1987).
[34] K. Teichmann, M. Wenderoth, S. Loth, R. Ulbrich, J. Garleff, A. Wijnheijmer, and P. Koenraad, Physical Review Letters 101, 076103 (2008).
[35] V. W. Brar *et al.*, Nature Physics 7, 43 (2011).
[36] C.-L. Song, Y.-P. Jiang, Y.-L. Wang, Z. Li, L. Wang, K. He, X. Chen, X.-C. Ma, and Q.-K. Xue, Physical Review B 86, 045441 (2012).
[37] S. Selçuk and A. Selloni, The Journal of Chemical Physics 141, 084705 (2014).
[38] G. Henkelman, B. P. Uberuaga, and H. Jónsson, The Journal of Chemical Physics 113, 9901 (2000).
[39] M. Dion, H. Rydberg, E. Schröder, D. C. Langreth, and B. I. Lundqvist, Physical Review Letters 92, 246401 (2004).
[40] G. Kresse and J. Furthmüller, Computational Materials Science 6, 15 (1996).
[41] A. A. Mostofi, J. R. Yates, G. Pizzi, Y.-S. Lee, I. Souza, D. Vanderbilt, and N. Marzari, Computer Physics Communications 185, 2309 (2014).
[42] J. P. Perdew, K. Burke, and M. Ernzerhof, Physical review letters 77, 3865 (1996).
[43] http://theory.cm.utexas.edu/vtsttools/neb.html.
[44] J. Sun, H. Shi, T. Siegrist, and D. J. Singh, Applied Physics Letters 107, 153902 (2015).

[45] T. Björkman, A. Gulans, A. V. Krasheninnikov, and R. M. Nieminen, Physical Review Letters 108, 235502 (2012).
[46] H.-P. Komsa, S. Kurasch, O. Lehtinen, U. Kaiser, and A. V. Krasheninnikov, Physical Review B 88, 035301 (2013).